Design, development and use of the spectrometer for investigating coherent THz radiation produced by micro-bunching instabilities at Diamond Light Source

2016 J. Phys.: Conf. Ser. 732 012039

(http://iopscience.iop.org/1742-6596/732/1/012039)

Design, development and use of the spectrometer for investigating coherent THz radiation produced by micro-bunching instabilities at Diamond Light Source

Aiveen Finn[1,2], **Pavel Karataev**[1], **Guenther Rehm**[2]

[1] JAI at Royal Holloway University of London, Egham, UK
[2] Diamond Light Source, Oxfordshire, UK

E-mail: aiveen.finn.2013@live.rhul.ac.uk

Abstract. Schottky barrier diodes (SBDs) are known for their low noise, ultra-fast response and excellent sensitivity. They are often implemented as detectors in the millimetre wavelength regime. Micro-bunch instabilities (MBI) have been detected at many light sources around the world including the Diamond Light Source, UK. These MBI can result in bursts of coherent synchrotron radiation (CSR) with millimetre wavelengths. More research needs to be carried out with regards to the dynamics of MBI in order to confirm the simulations and to eventually harness the power of the CSR bursts. A single shot spectrometer has been designed and is under operation at the Diamond Light Source (DLS). It is composed of eight SBDs ranging from 33-1000 GHz. Unlike previous measurements carried out, each of the SBDs has been individually characterised thus making the results obtained comparable to simulations. In this paper, we present the assessment of each SBD in the spectrometer and the first results of the spectrometer's use in the beam.

1. Introduction

MBI occur when the single bunch charge exceeds a threshold current and the bunch begins to filament [1]. The filaments proceed to emit CSR which is of mm-wavelengths at DLS. CSR only occurs at wavelengths longer than the bunch unless their emission is shielded. However, when the CSR is caused as a result of MBI, the wavelength of CSR can occur at wavelengths shorter than the bunch length. It is important to note that the wavelength of CSR is limited by the longitudinal electron bunch dimension and must be longer than the beam filament emitting it (coherent emission), but the wavelength is usually much shorter than the overall bunch length.

DLS along with other light sources across the globe have observed micro-bunch instabilities [2–7]. Correspondingly, MBI and their resulting CSR bursts are monitored and investigated worldwide utilising different methods and instruments. The approach undertaken here is to investigate these instabilities in a turn-by-turn regime in order to measure the spectral characteristics of the CSR and compare with simulations. A single shot spectrometer has been developed with each of the detectors it contains characterised in order to thoroughly analyse the data.

2. Schottky Detector Diodes

Schottky Barrier Diodes (SBDs) are able to detect mm-waves at room temperature and hence are often used as detectors within this wavelength range. Their main attributes are low noise, excellent sensitivity and fast responses [8]. SBDs are versatile and can be operated so as to fit a specific application, when terminated with a low impedance (typically 50 Ω) the SBDs operate at a much faster speed but at the cost of lower sensitivity. In the set-up as described in this paper, the SBDs are connected to a high impedance (10 kΩ in this case) and thus achieve a higher sensitivity at a compromise of slower speed.

Of the eight detectors chosen, seven are housed within waveguides and fed signal via horn antennas. The eighth detector is a broadband quasi-optical detector (QOD) with a silicon lens. All eight SBDs are in a high impedance set up (10 kΩ) to take full advantage of the high sensitivity. Each detector and its corresponding horn antenna (where applicable) have been individually characterised on the test bench. Consequently, a spectrometer has been designed using eight SBDs, with each detector covering a specific frequency band from 33-1000 GHz. The three detectors with the lower frequency ranges are supplied by Millitech Inc, USA, while the remaining five detectors are from Virginia Diodes Inc, USA. Table 1 shows the properties of the chosen SBDs.

Table 1. SBD Specifications

Detector Model	Stated Range	Waveguide Range
DXP-22 [9]	33 - 50 GHz	26.36 - 52.73 GHz
DXP-12 [9]	60 - 90 GHz	48.41 - 96.81 GHz
DET-08 [9]	90 - 140 GHz	73.82 - 147.64 GHz
WR5.1ZBD [10]	140 - 220 GHz	115.79 - 231.59 GHz
WR3.4ZBD [10]	220 - 330 GHz	173.69 - 347.38 GHz
WR2.2ZBD [10]	330 - 500 GHz	295.28 - 590.55 GHz
WR1.5ZBD [10]	500 - 750 GHz	393.70 - 787.40 GHz
QOD [10]	100 - 1000 GHz	n/a (silicon lens)

3. Test Bench Set Up

A Thomas Keating (TK) Power Meter was used to characterise both the source and thus the individual detectors. It is a broadband detector requiring modulated signal. The main benefit of the TK power meter is that it can be calibrated by injecting a known amount of power electrically into the instrument. As a result of this, the TK power meter can then be used to quantify the source (on the test bench) and therefore the SBDs too.

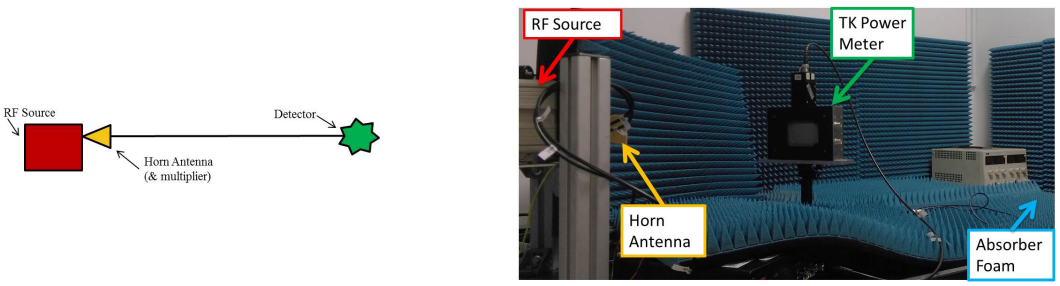

Figure 1. A schematic and photograph of the Test Bench set-up.

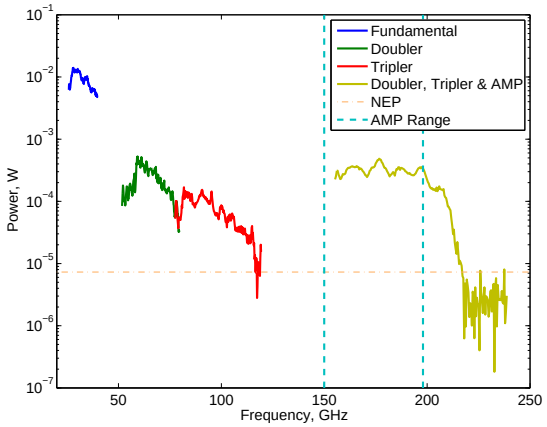

Figure 2. Power of signal received by the TK power meter for 26 - 240 GHz at a distance of 50 cm from the source with amplification on the doubler-tripler combination. NEP is the calculated Noise Equivalent Power of the TK within the described set-up.

The Ka band emitter (26.5 - 40 GHz) is the radio frequency (RF) source used on the test bench (figure 1) to produce a signal with which the detectors are quantified. The emitter employs a Gunn diode to produce the output frequency. In order to achieve the desired frequency ranges, various multipliers were utilised. The properties of the multipliers are show in table 2. Due to the nature of multipliers, the strength of the signal unceasingly declines when passing through one (or more). To counteract this continual decrease in signal, an amplifier was used to boost the output power. The amplifier utilised is an AMP-15 from Millitech Inc, USA with an input frequency of 50 - 66 GHz and a gain of 22 dB.

Table 2. Frequency Multipliers

Model	**Type**	**Output Frequency**
MUD-15 [9]	Doubler	50 - 75 GHz
MUT-10 [9]	Tripler	75 - 110 GHz
WR5.1X3 [11]	Tripler	140 - 220 GHz

First, the TK power meter was calibrated and using this information the RF source was quantified over the entire range of frequencies using the multipliers and amplifier (26 - 240 GHz). In figure 2, the power of the signal received by the TK head over the range of frequencies can be seen. In order to minimise reflections, the area in and around the test bench was lined with pyramidal absorber and the TK head was placed at Brewster's angle with respect to the source, 55.5°. The distance of 50 cm was decided upon to ensure the SBDs would receive sufficient signal but would not be saturated. Despite the source and combination of multipliers achieving frequencies higher than 240 GHz, due to the limited range of the amplifier approximately 30 GHz of the 240 GHz occurs below the NEP. Therefore, this cannot be used with regards the characterisation and thus the enforced upper limit of the set-up becomes 217 GHz.

4. Characterisation of Detectors

A power density approach was taken in order to determine the responsivities of each detector and its particular horn antenna combination. The aperture of the TK is large, especially in contrast to the physical apertures of the individual horn antennas, thus by calculating sensitivities with

respect to area a more applicable result was obtained. Furthermore, the sensitivities determined from the power densities have been calculated for the detector and horn antenna combination in the forward direction. For every detector and horn antenna combination displayed here, the fundamental (i.e. TE_{10}) mode cut off of the waveguide is depicted as well as the lower cut off of the frequency of the next mode.

From figure 3, it can be seen that the sensitivity across the frequency range of DXP22 is quite constant. After the lower cut off of the next mode, the detector is still able to observe signal albeit erratically. This is to be expected because once dealing with higher modes it is difficult to predict what will happen with respect to the power in the waveguide. With regards DXP12

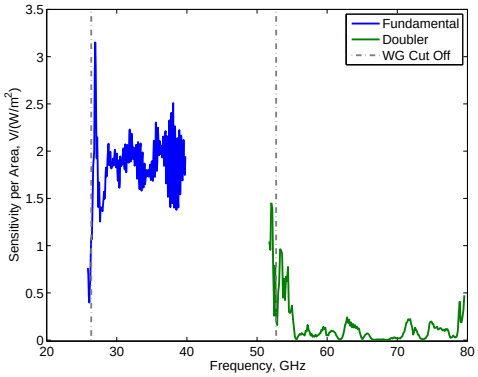

Figure 3. The sensitivity per unit area for DXP22 (33 - 50 GHz).

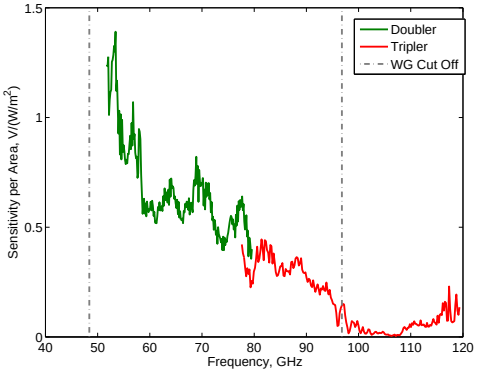

Figure 4. The sensitivity per unit area for DXP12 (60 - 90 GHz).

shown in figure 4, the sensitivity per area decreases with an increase of frequency. There is a clear overlap between the signal observed with the doubler and the tripler. Though signal is detected after the waveguide boundary, it is with a lower sensitivity per area. The shape of the curve of DET08 in figure 5, contrasts greatly with the previous figures from fellow detectors by Millitech Inc. DET08 has a peak sensitivity per area at 100 GHz.

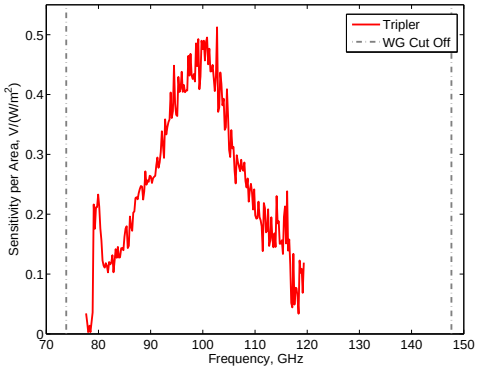

Figure 5. The sensitivity per unit area for DET08 (90 - 140 GHz).

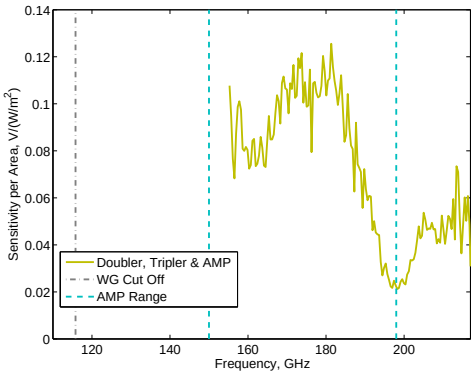

Figure 6. The sensitivity per unit area for WR5.1 (140 - 220 GHz).

As seen in figure 7, the sensitivity of WR3.4 is extremely fluctuating. There are two main points of change, the first is at and after the lower cut off of the waveguide and then again after the fall off from the power amplifier.

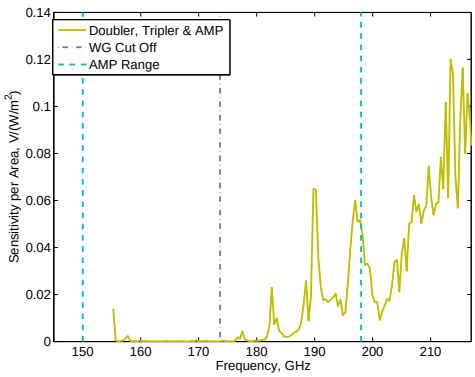

Figure 7. The sensitivity per unit area for WR3.4 (220 - 330 GHz).

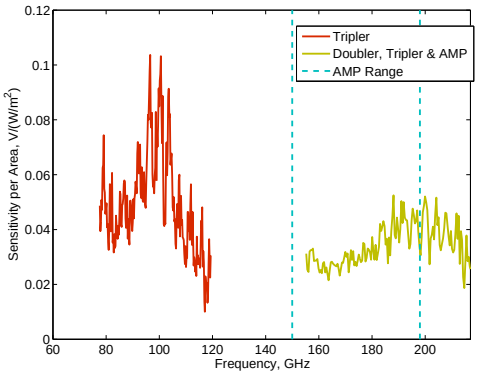

Figure 8. The sensitivity per unit area for Quasi-Optical Detector (100 - 1000 GHz).

The QOD is not housed within a waveguide, but rather a silicon lens to guide the signal into an antenna. The range as stated by the manufacturer of the QOD is 100 - 1000 GHz and it is clear that from probing the lower end of the frequencies the sensitivity is not uniform. As shown in figure 8, the sensitivity fluctuates a lot within the frequency ranges. The variability in the sensitivities can be attributed to the silicon lens being of the same or similar size as the wavelength thus causing standing waves.

The remaining detectors (WR2.2 and WR1.5) and the higher frequencies of already mentioned detectors will be further quantified using a THz laser.

5. Spectrometer/Detector Array

The spectrometer has been created in such a manner that all eight SBDs are as close together as possible to observe the most signal simultaneously (figure 9). In order to eliminate the risk of shadowing all entrance apertures are in one plane. Due to the nature of waveguides, the horn antennas and hence detectors must be aligned correctly in order to observe the E-field.

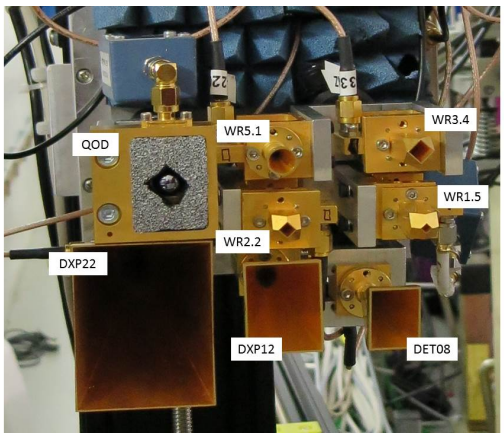

Figure 9. Layout of detector array plate.

Within the Diamond Storage Ring tunnel, there is a viewport that has been dedicated to the investigations of CSR from MBI [12]. The viewport transports the synchrotron radiation from dipole B06 to the silica viewport window (figure 10). The distance travelled is approximately

3.5 metres, whereby the radiation travels parallel but vertically lower than the electron beampipe. In order to alter the path of the desired radiation, copper mirrors are brought into play. These water-cooled mirrors not only guide the mm-radiation through the viewport but also absorb the x-ray radiation which is created by the dipole magnet and usually required by beamlines at DLS.

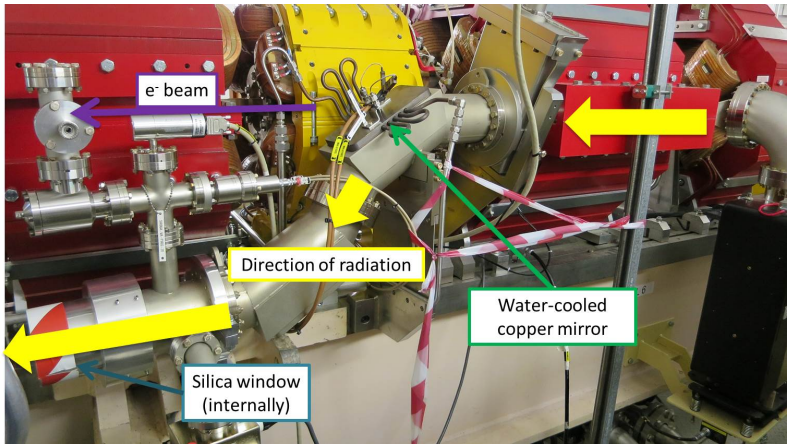

Figure 10. The path the radiation takes within the viewport from just after B06 to the silica window.

As shown in figure 11, the detector plate is installed in open air in front of the silica window, not further than 1 metre away. The detector array plate is attached to a three-way motion set up in order to move the spectrometer in the x-, y- and z-plane and thus to optimise the signal obtained in the different channels. Directly after the viewport window is a sheet of styrofoam, which is used to block unwanted frequencies that may affect the measurements, namely visible wavelengths of light and infrared while allowing THz and mm-wavelengths to pass through.

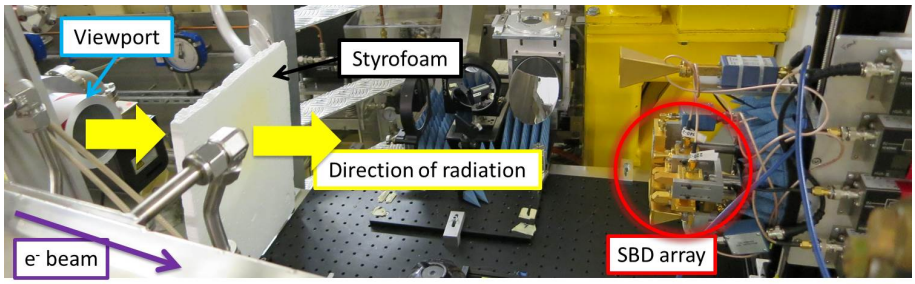

Figure 11. The detector array installed in the tunnel with respect to the viewport.

6. Data Analysis

The signals from the eight channels are individually amplified before being carried out of the tunnel via coaxial cables to be analysed. The amplifiers (FEMTO, Germany HVA-S Switchable Gain) are used to boost the signal above the noise, because otherwise the distanced travelled by the signals is great (less 30 m) and the signals would become engulfed by noise.

The amplifiers connected to each of the SBDs have a high input impedance so that the SBDs achieve a high sensitivity rating. The input impedance of the amplifiers is 10 kΩ and because we are working in the high impedance regime, the capacitance of the cables becomes very important.

The effect of capacitive loading of the cables can be altered by choosing shorter cables and using cables with a lower capacitance. In the set-up described here, cables with a lower capacitance were employed, but the primary contribution was that the amplifiers are mounted close to the detector array, to minimise cable length.

The signals are amplified and then travel along approximately 30 metres of cables until they reach the simultaneous multichannel digitiser. The ADC is a d-tAcq ACQ425ELF with a sampling rate of 1 MSPS and the possibility for 16 input channels. It constantly streams out the data where it is fed into a local computer. This computer carries out FFTs of the data, selects the region of interest and executes a power average over every ten data sets. The region of interest is focussed around the revolution frequency (533.820 kHz) of the synchrotron storage ring, as opposed to DC. SBDs produce flicker noise, which has a 1/f power spectrum, so the signal to noise on their readout will be better when at higher frequency. As Nyquist sits at 500 kHz, the frequency range is imposed to be 33.820 kHz symmetrically either side of the central frequency.

7. MBI Observations

Since its installation in the storage ring, the SBD array has been capturing data. The data presented here was obtained when the storage ring was set to user optics with a single bunch fill [13]. When the RF cavities had a combined voltage of 2.2 MV, a single bunch was injected into the storage ring with a low current of just 1.07 mA. Slowly the current was increased to 4.15 mA. It was not possible to inject more charge into the single bunch, as this caused the bunch to become unstable and the beam was kicked out of the storage ring. During the current ramp of 1.07 mA to 4.15 mA, data was continually obtained and the bursting of MBI observed. In figure 12, the signal obtained at the revolution frequency (533.820 kHz) is displayed for each

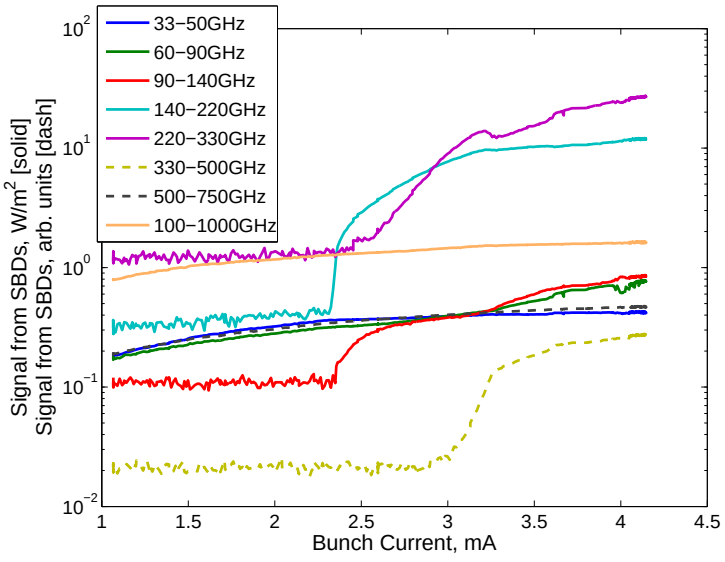

Figure 12. The signal obtained by the SBDs and depicted as the power for a unit area.

of the eight detectors. As only six of the eight detectors were characterised, the remaining two detectors (WR2.2 (330 - 500 GHz) and WR1.5 (500 - 750 GHz)) have dashed lines to represent the different units. Figure 13 depicts the signal observed solely in the sidebands i.e. within the ± 33.820 kHz range excluding the central frequency for each detector. The activity occurring either side of the revolution frequency was termed the 'variation' or 'noise' because it only occurs with bursting or disturbances in the ring. The variation in most cases remains quite constant.

Finally, in figure 14 the relationship between the signal at revolution frequency and its variation can be observed.

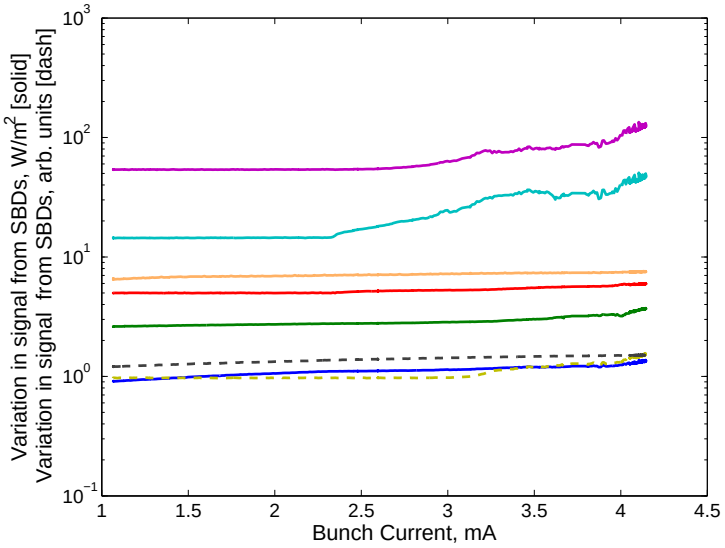

Figure 13. The variation in each of the channel's signals, whereby the variation could be interpreted as the standard deviation.

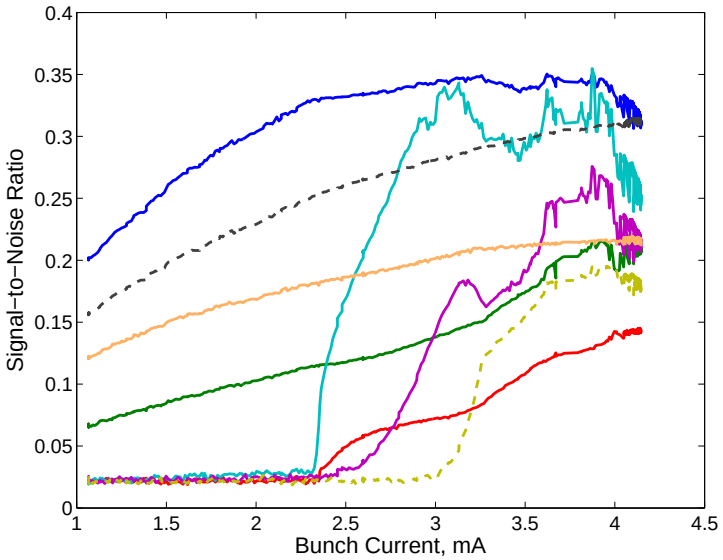

Figure 14. The ratio between figure 12 and figure 13 is depicted.

DXP22 (33 - 50 GHz) portrays a smooth signal and variance, this is due to its low(er) frequency view where there is less change than for the higher frequency detectors to observe. Furthermore, the broadband QOD can probe the higher frequencies but because of the strong and constant signal from the DXP22, the QOD becomes overpowered by this lower frequency signal and thus they achieve similar curves shapes. It is clear to see from the data obtained, WR5.1 (140 - 220 GHz) and WR3.4 (220 - 330 GHz) observed the most amount of signal. This

is extremely obvious in figure 12 where the power they observe is at least an order of magnitude above the rest. These two detectors also have the most variance (figure 13) and thus incur an erratic ratio (figure 14). In figure 14, there is a sudden change at 2.3 mA representing the lengthening of the bunch. This value of 2.3 mA for these machine parameters could thus be declared as the bursting threshold.

8. Conclusions & Future Plans

The data presented here show that six of the eight detectors were characterised on the test bench, thus allowing for quantitative analysis when using the detector array in the beam at DLS. As the source and accompanying multipliers can only generate frequencies with sufficient power up to 217 GHz, the SBDs requiring higher frequencies will be quantified using a terahertz laser.

The initial results from experiments taken at DLS are depicted here and for the first time the results are presented as real units (W/m^2) and not arbitrary units.

A full analysis of raster scans will be undertaken so that a location favourably suitable for all eight detectors can be determined for its placement in the storage ring tunnel with respect to the viewport silica window. Following on from this determination, further data will be taken at DLS and thus analysis carried out. Future experiments at DLS include obtaining data under various beam condition in particular 'Low Alpha modes', when the momentum compaction factor is set to be small [14].

References

[1] Venturini M, Warnock R, Ruth R and Ellison J 2005 *Phys. Rev. ST Accel. Beams* **8** 014202
[2] Abo-Bakr M, Feikes J, Holldack K, Wüstefeld G and Hübers H W 2002 *Phys. Rev. Lett.* **88** 254801
[3] Rehm G, Morgan A F, Bartolini R, Martin I P S and Karataev P 2009 *Proc. of DIPAC* (Basel, Switzerland) pp 369–371
[4] Podobedov B, Carr G L, Kramer S L and Murphy J B 2001 *Proc. of Particle Accelerator Conf.* vol 3 (Chicago, IL, USA) pp 1921–1923
[5] Byrd J M, Leemans W P, Loftsdottir A, Marcelis B, Martin M C, Mckinney W R, Sannibale F, Scarvie T and Steier C 2002 *Phys. Rev. Lett.* **89** 224801
[6] Mochihashi A, Hosaka M, Katoh M, Shimada M and Kimura S 2006 *Proc. of EPAC* (Edinburgh, Scotland) pp 3380–3382
[7] Kuske P 2009 *Proc. of Particle Accelerator Conf.* (Vancouver, BC, Canada) pp 4682–4684
[8] Smith R J and Dorf R C 1992 *Circuits, Devices and Systems* 5th ed (John Wiley & Sons Inc.)
[9] Millitech Inc. *Detector Specifications* URL `http://www.millitech.com/`
[10] Virginia Diodes Inc. *VDI User Guide* URL `http://vadiodes.com/index.php/en/`
[11] Virginia Diodes Inc. *VDI User Guide WR5.1 WR3.4 WR2.2* URL `http://vadiodes.com/index.php/en/`
[12] Shields W, Boorman G and Karataev P 2012 *Proc. of IPAC* (New Orleans, Louisiana, USA) pp 3114–3116
[13] CCLRC 2002 *Diamond Synchrotron Light Source: Report of the Design Specification*
[14] Martin I P S, Rehm G, Thomas C and Bartolini R 2011 *Phys. Rev. ST Accel. Beams* **14** 040705